ORIGINAL ARTICLE

Basic Study

Evaluation of therapeutic effectiveness of 131I-antiEGFR-BSA-PCL in a mouse model of colorectal cancer

Wei Li, Yan-Hui Ji, Cheng-Xia Li, Zhong-Yun Liu, Ning Li, Lei Fang, Jin Chang, Jian Tan

Wei Li, Yan-Hui Ji, Cheng-Xia Li, Ning Li, Jian Tan, Department of Nuclear Medicine, Tianjin Medical University General Hospital, Tianjin 300052, China

Zhong-Yun Liu, Yantai Institute of Coastal Zone Research, Chinese Academy of Sciences, Yantai 264003, Shandong Province, China

Lei Fang, Jin Chang, Institute of Nanobiotechnology, School of Materials Science and Engineering, Tianjin Key Laboratory of Composites and Functional Materials, Tianjin University, Tianjin 300072, China

Institutional animal care and use committee statement: This study was performed in accordance with the guidelines of the National Institutes of Health Guide for the Care and Use of Laboratory Animals and was approved by the Animal Care and Use Committee of Tianjin Medical University.

Conflict-of-interest statement: To the best of our knowledge, no conflict of interest exists.

Data sharing statement: The technical appendix, statistical code, and dataset are available from the corresponding author at (tanpost@163.com). Participants gave informed consent for data sharing. The authors confirm that all data underlying the findings are fully available without restriction. All relevant data are mentioned in the paper. No additional data are available.

Correspondence to: Jian Tan, MD, Professor of Medicine, Chief, Department of Nuclear Medicine, Tianjin Medical University General Hospital, Anshan Road 154, Heping District, Tianjin 300052, China. tanpost@163.com
Telephone: +86-22-60362881

Abstract

AIM: To investigate the biological effects of internal irradiation, and the therapeutic effectiveness was assessed of 131I-labeled anti-epidermal growth factor receptor (EGFR) liposomes, derived from cetuximab, when used as a tumor-targeting carrier in a colorectal cancer mouse model.

METHODS: We described the liposomes and characterized their EGFR-targeted binding and cellular uptake in EGFR-overexpressing LS180 colorectal cancer cells. After intra-tumor injections of 74 MBq (740 MBq/mL) 131I-antiEGFR-BSA-PCL, we investigated the biological effects of internal irradiation and the therapeutic efficacy of 131I-antiEGFR-BSA-PCL on colorectal cancer in a male BALB/c mouse model. Tumor size, body weight, histopathology, and SPECT imaging were monitored for 33 d post-therapy.

RESULTS: The rapid radioiodine uptake of ^{131}I-anti-EGFR-BSA-PCL and ^{131}I-BSA-PCL reached maximum levels at 4 h after incubation, and the ^{131}I uptake of ^{131}I-antiEGFR-BSA-PCL was higher than that of ^{131}I-BSA-PCL *in vitro*. The ^{131}I tissue distribution assay revealed that ^{131}I-antiEGFR-BSA-PCL was markedly taken up by the tumor. Furthermore, a tissue distribution assay revealed that ^{131}I-antiEGFR-BSA-PCL was markedly taken up by the tumor and reached its maximal uptake value of 21.0 ± 1.01 %ID/g (%ID/g is the percentage injected dose per gram of tissue) at 72 h following therapy; the drug concentration in the tumor was higher than that in the liver, heart, colon, or spleen. Tumor size measurements showed that tumor development was significantly inhibited by treatments with ^{131}I-antiEGFR-BSA-PCL and ^{131}I-BSA-PCL. The volume of tumor increased, and treatment rate with ^{131}I-antiEGFR-BSA-PCL was 124% ± 7%, lower than that with ^{131}I-BSA-PCL (127% ± 9%), [131]I (143% ± 7%), and normal saline (146% ± 10%). The percentage losses in original body weights were 39% ± 3%, 41% ± 4%, 49% ± 5%, and 55% ± 13%, respectively. The best survival and cure rates were obtained in the group treated with ^{131}I-antiEGFR-BSA-PCL. The animals injected with ^{131}I-antiEGFR-BSA-PCL and ^{131}I-BSA-PCL showed more uniform focused liposome distribution within the tumor area.

CONCLUSION: This study demonstrated the potential beneficial application of ^{131}I-antiEGFR-BSA-PCL for treating colorectal cancer. ^{131}I-antiEGFR-BSA-PCL suppressed the development of xenografted colorectal cancer in nude mice, thereby providing a novel candidate for receptor-mediated targeted radiotherapy.

Key words: Radioiodine therapy; Colorectal cancer; Liposome; Epidermal growth factor receptor; Mouse

Core tip: This paper describes liposomes that were assessed for EGFR-targeted binding and cellular uptake in EGFR-overexpressing LS180 colorectal cancer cells and a mouse model of colorectal cancer. Anti-EGFR and non-targeted liposomes were labeled with ^{131}I using the chloramine-T method. The time-dependent cellular uptake of ^{131}I-antiEGFR-BSA-PCL and ^{131}I-BSA-PCL demonstrated the slow-release effects of nanoparticles. The results of confocal microscopic analysis revealed the significant uptake of antiEGFR-BSA-PCL in LS180 cells. This study also investigated the biological effects of internal irradiation and the therapeutic efficacy of ^{131}I-antiEGFR-BSA-PCL on colorectal cancer in a BALB/c mouse model. To address this issue, tumor size, body weight, histopathology, and SPECT imaging were monitored for 33 d post-therapy. The ^{131}I-antiEGFR-BSA-PCL was demonstrated to be superior in regard to cellular binding and uptake compared with control BSA-PCL in the mouse model.

INTRODUCTION

Cancer is a major threat to public health in the 21st century and one of the leading causes of death worldwide. However, the mechanisms of carcinogenesis, cancer invasion, and metastasis remain unclear[1]. Colorectal cancer is the third most common cancer worldwide. Approximately 25% of patients with colorectal cancer present with overt metastatic disease; metastatic disease develops in 40% to 50% of newly diagnosed patients[2]. The clinical need for image-based detection and monitoring for effective therapeutic management to reduce the mortality caused by this disease has not been met to date. Therefore, novel strategies and treatment concepts are needed, particularly because conventional cancer therapies, such as external radiation and chemotherapy, have problems such as poor specificity. These conventional therapies often cause dose-limiting side effects and inhibit the possibility of curative treatments.

Nanomedicine has exploited the possibility of designing tumor-targeted nanocarriers that can deliver radionuclide payloads in a site- or molecule-selective manner based on their magnetic properties, thereby improving the effectiveness and safety of cancer molecular imaging and therapies. Many studies have proven the feasibility of the use of targeted nanoparticle probes. Nanotechnology can lead to fundamental changes and improve the current understanding of biological processes in health and disease as well as enable novel diagnostics and therapeutics for treating cancer; consequently, advances made on the basis of nanotechnology could lead to progress in healthcare[3]. Targeted drug delivery systems, such as passive and active targeting nanoparticles or nanocarriers, have been developed to improve the biodistribution, pharmacological, therapeutic, and toxic properties of chemical agents used in cancer diagnostics and therapeutics[4]. The abundant expression and signal amplification properties of these targets are mandatory for successful receptor-targeted tumor imaging and for their subsequent clinical translation[5]. The epidermal growth factor receptor (EGFR) is a transmembrane receptor belonging to the ErbB family of receptors; the EGFR family includes four transmembrane receptors, namely, EGFR, HER2, HER3, and HER4[6]. EGFR is a cell surface receptor that plays a key role in signaling pathways, and such pathways regulate cell proliferation, angiogenesis, and tumor metastasis[7,8]. Previous studies reported that EGFR is widely overexpressed

in several tumor types, including breast cancer, melanoma, brain glioblastoma, non-small cell lung cancer[9], and colorectal cancer[10]; thus, EGFR is an attractive candidate for anti-cancer therapy.

Several radionuclides have been surface-bioconjugated or after-loaded in nanoparticles to improve their effectiveness and reduce the toxicity of cancer imaging and therapies in preclinical and clinical studies. In the broad spectrum of available radionuclides, beta emitters such as ^{90}Y, ^{131}I, and ^{177}Lu are the most commonly used for targeted therapies[11]. [131]I provides imaging feasibility and beta-emitting therapeutic effects[12]. The application of nanotechnology for the diagnosis and treatment of colorectal cancer has the potential to improve conventional methods as well as help with the development of novel approaches for detection and therapy[13].

In the present study, ^{131}I-antiEGFR-BSA-PCL and ^{131}I-BSA-PCL were successfully synthesized. These liposomes were characterized for cellular uptake, time-dependent uptake of ^{131}I by LS180 cells *in vitro*, therapeutic efficacy, histopathology, tissue distribution, and SPECT imaging in an LS180 xenografted nude mouse model.

MATERIALS AND METHODS

Materials
The following reagents and materials used in this study were obtained: Minimum Essential Medium Eagles with Earle's Balanced Salts (MEM-EBSS; Gibco), fetal bovine serum (FBS; Gibco), rabbit polyclonal anti-human epidermal growth factor receptor antibody (Abcam, ab2430), 5 mg/mL monoclonal antibody (MERCK Inc., C225; cetuximab), and PV-6000 Polymer Detection System (ZSGB-BIO Co.).

Cell line
The colorectal cancer cell line LS180 was purchased from the Cell Resource Center, Institute of Basic Medical Sciences, Chinese Academy of Medical Sciences/Peking Union Medical College (Beijing, China). The cells were maintained in MEM-EBSS medium supplemented with 10% FBS and 1% penicillin/streptomycin. The LS180 cells were grown at 37 ℃ in a humidified incubator with a mixture of 95% air and 5% CO2.

Preparation of nanoparticles
The cetuximab-decorated, BSA-PCL-conjugated antiEGFR-BSA-PCL and BSA-PCL liposomes were synthesized by the researchers from the Department of Polymer Materials Science and Engineering of Tianjin University[14]. The antiEGFR-BSA-PCL and BSA-PCL liposomes were labeled with [131]I (Beijing Atomic Hi-tech Co., Ltd.) *via* the chloramine T method. A detailed description and biological characterization of the compounds are presented by Ickenstein *et al*[15]. The labeling rate and the radiochemical purity

of ^{131}I-labeled nanoparticles were determined by thin layer chromatography.

Liposomal targeting in EGFR-overexpressing LS180 cells
The cellular binding and uptake of the antiEGFR-BSA-PCL and BSA-PCL liposomes were evaluated by confocal microscopy in LS180 cells. The antiEGFR-BSA-PCL and BSA-PCL liposomes were first labeled by fluorescein isothiocyanate (FITC), then were added at a concentration of 1 mg/10^6 cells. The cell cultures were then incubated for 4 h at 37 ℃. After incubation, cells were washed thrice with PBS, fixed with 4% paraformaldehyde, and analyzed by confocal microscopy (laser scanning confocal microscope, Olympus FV1000; Japan).

Time-dependent cellular uptake of ^{131}I-antiEGFR-BSA-PCL and ^{131}I-BSA-PCL
To evaluate the time-dependent cellular uptake of ^{131}I-antiEGFR-BSA-PCL and ^{131}I-BSA-PCL, approximately 1 × 10^5 cells per well were seeded in 96-well plates and cultured with 0.37 MBq/mL to 3.7 MBq/mL ^{131}I-antiEGFR-BSA-PCL and ^{131}I-BSA-PCL for 4 h. The medium was completely removed before the cells were washed and lysed twice with ice-cold PBS. Subsequently, 200 μL of DMEM containing 10% FBS was added into each well. The cells were counted every 2 h until 24 h of incubation. Radioactivity was measured with a γ counter (LKB gamma 1261; LKB Instruments, Waverley, Australia) to calculate the counts per minute (CPM) after 24 h. All of these experiments were performed in triplicate.

Animal model
Experimental subjects were four-week-old BALB/c female nude mice weighing 9 g to 11 g. These mice were purchased from the Beijing Experimental Animal Center of Peking Union Medical, China. Mice were kept under specific pathogen-free conditions, with a constant temperature of 25 ℃ to 27 ℃ and a constant humidity of 45% to 50% in the Laboratory Animal Center of the Tianjin Medical University, China. Animal experimentation guidelines were followed according to the regulations of Swiss veterinary law. The LS180 tumor cells, with approximately 1 × 10^7 cells per 50 μL, were subcutaneously injected into the right flank of the mice. According to the principle of the human thyroid perchlorate discharge test, 0.05 mg/mL sodium perchlorate was added to the drinking water of all mice for 1 d before the experiment (approximately 21 d after tumor inoculation) to reduce the exposure of their thyroids to unwanted radiation and imaging. The growth curve experiment was terminated at 54 d after tumor inoculation, and all the mice were sacrificed. When tumor volume reached an average size of 1.0 cm^3, mice were randomly divided into four experimental groups, which were subjected to

an intra-tumor injection of 74 MBq (740 MBq/mL) ^{131}I-antiEGFR-BSA-PCL, ^{131}I-BSA-PCL, ^{131}I, or an equivalent volume of normal saline (except in the SPECT imaging experiment).

Tissue distribution of ^{131}I, ^{131}I-antiEGFR-BSA-PCL, and ^{131}I-BSA-PCL

The mice bearing human colorectal cancer were used for the biodistribution study at day 21 after tumor inoculation. The mice in each group were sacrificed at 4, 24, and 72 h post-injection of drugs, respectively. The heart, spleen, liver, colon, and tumor samples were collected for weighing and for radio-activity measurements with a γ counter (LKB gamma 1261; LKB Instruments). %ID/g represents the percentage injected dose per gram of tissue. %ID/g was determined by the percentage of radioactivity contained within each gram of tissue compared to the total radioactivity injected into the body[16,17]. Meanwhile, the remaining spleen, liver, and tumor tissues were collected to study the histopathology of each group.

Therapeutic efficacy studies

Toxicity was monitored by measuring the body weight and tumor volume. During the course of treatment, the animal body weight and *in vivo* tumor growth were measured at day 21 after tumor cell inoculation. Mice were checked for survival every day; their body weight and tumor volume were measured every 3 d until the end of the study. The growth curve experiment was terminated at 54 d after tumor inoculation, and all mice were then sacrificed. After treatment, the length, width, and height of the tumors were measured with calipers once every 3 d. Tumor volume was calculated as follows: volume = $1/6 \times \pi \times$ length (cm) × width (cm) × height (cm)[18].

Histopathology studies

The xenografted colorectal cancer cell line LS180 was characterized for EGFR overexpression by immunohistochemistry. For the immunohistochemical staining of EGFR, the rabbit polyclonal anti-human EGFR antibody (1:500) was used as the primary antibody, followed by PV 6000 *via* the two-step immuno-histochemical detection of cell-associated EGFR. Mice from each group were sacrificed at 4, 24, and 72 h after the injection of different liposomes. The remaining spleen, liver, and tumor tissues were collected to study their histopathology. The organs from the four groups were dissected, fixed in 10% formalin for 48 h, embedded in paraffin, and sectioned. The sections (5-6 μm) were then stained with hematoxylin and eosin. The histopathological changes of the tissue were ultimately examined using light microscopy (Olympus × 40).

SPECT whole-body imaging

For the SPECT imaging (Discovery VH 670; GE, United States), mice from the three treatment groups (except for the normal saline group) received an intra-tumor injection of 74 MBq (740 MBq/mL) of ^{131}I-antiEGFR-BSA-PCL, ^{131}I-BSA-PCL, and ^{131}I, respectively[19]. SPECT imaging was performed at 4, 24, and 72 h after injection.

Animal care and use statement

We ensured that mouse use was conducted in accordance with the highest scientific, humane, and ethical principles and was in compliance with regulations. We also ensured that housing conditions and care were species appropriate and that the environment was safe and secure for both animals and staff.

Statistical analysis

All *in vitro* experiments were performed in triplicate unless otherwise indicated. Statistical analyses were conducted with the SPSS software (version 17.0). The results are presented as the mean ± SD. Statistical significance was tested using Student's *t*-test or ANOVA, and *P*-values < 0.05 were considered statistically significant.

RESULTS

Basic properties of ^{131}I-BSA-PCL and ^{131}I-antiEGFR-BSA-PCL

The dynamic light scattering measurement showed that the average diameter of ^{131}I-BSA-PCL and ^{131}I-antiEGFR-BSA-PCL was approximately 180 nm, and the polydispersity index was 0.164, in agreement with the TEM result. The mean ζ potential of the obtained protein-based vesicle was also measured and was found to be -38.70 mV. The negative surface charge that resulted from the BSA shell could reduce undesired protein adsorption and provide good protection for the vesicle during the circulation in the body. The specific radioactivity was approximately 370-690 MBq/mg for ^{131}I-antiEGFR-BSA-PCL and ^{131}I-BSA-PCL. The labeling rate of ^{131}I was approximately 50%-85%, and the radiochemical purity was 95%-98%.

Internalization of EGFR-BSA-PCL and BSA-PCL

The effective diameter of BSA-PCL and antiEGFR-BSA-PCL was approximately 180 nm[14]. To assess the binding of antiEGFR-BSA-PCL and BSA-PCL to LS180 cells with EGFR overexpression, confocal microscopy was used. The confocal images and the immuno-fluorescence results of the LS180 cells incubated with antiEGFR-BSA-PCL and BSA-PCL were compared (Figure 1). antiEGFR-BSA-PCL was significantly internalized in the LS180 cells, which was shown by the appearance of strong green fluorescence. Compared with antiEGFR-BSA-PCL, BSA-PCL could similarly bind to cells, but the tumor retention was minimal, and the binding green fluorescence was weaker. This result suggests that the targeting ability of antiEGFR-BSA-PCL to tumor cells was enhanced by EGFR modification.
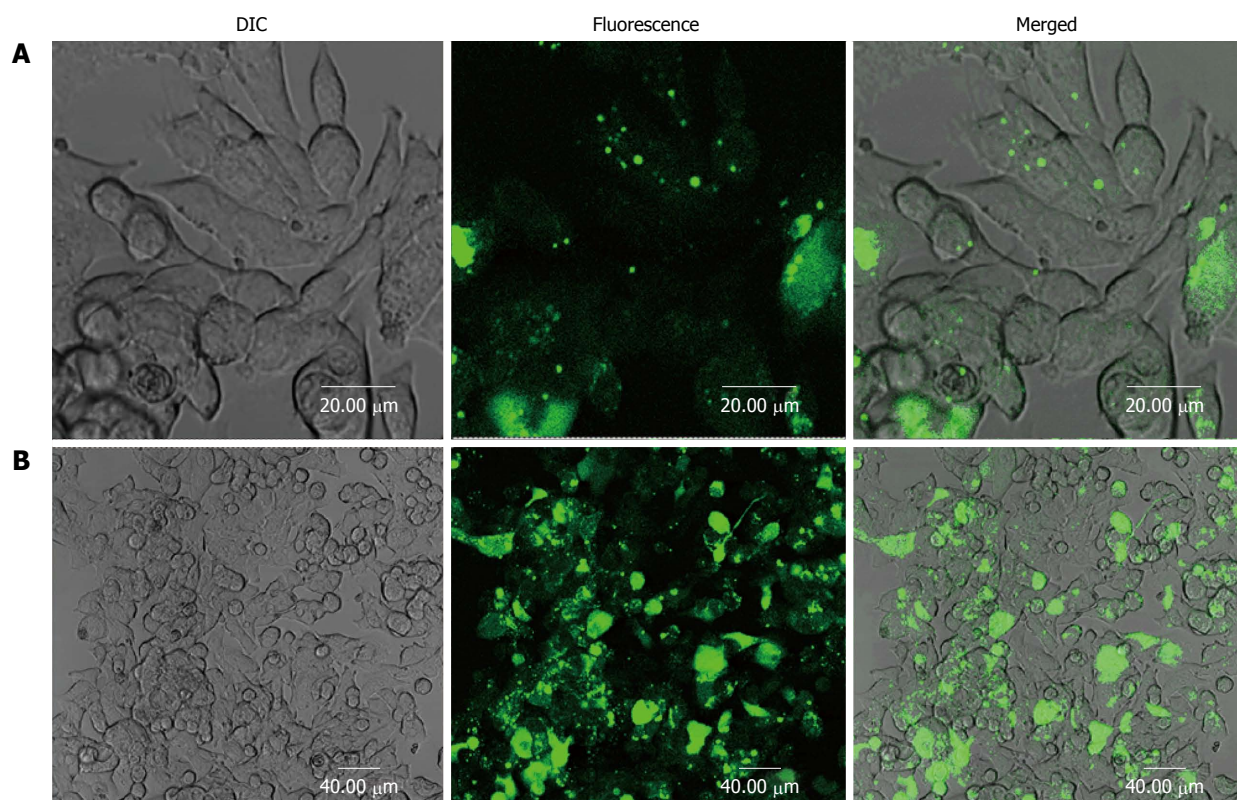
Figure 1 Confocal microscopy of LS180 cancer cells incubated with FITC-BSA-PCL and FITC-antiEGFR-BSA-PCL for 4 h.
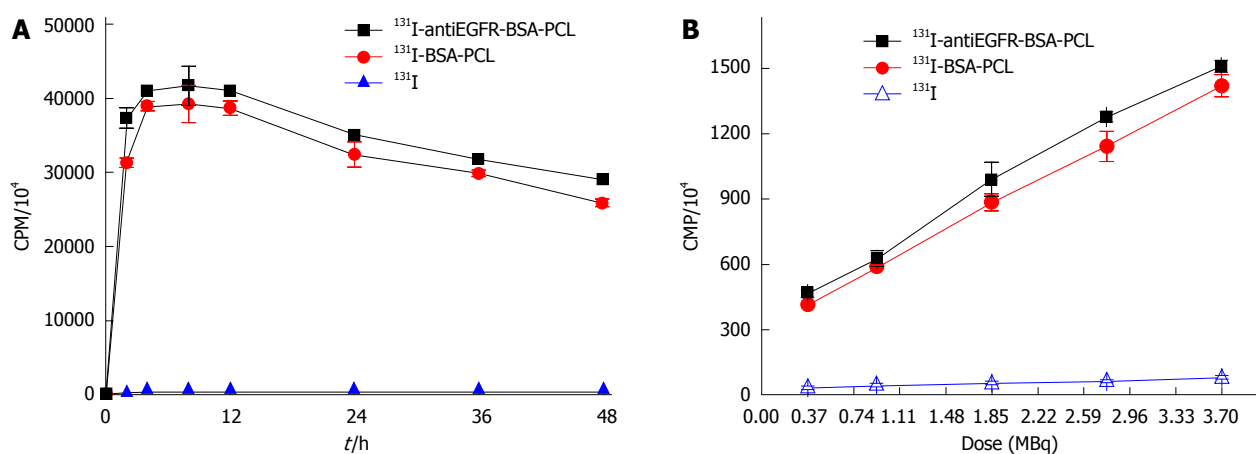

Figure 2 ^{131}I uptake in LS180 cells.

Time-dependent cellular uptake of ^{131}I-antiEGFR-BSA-PCL and ^{131}I-BSA-PCL

To determine the iodide uptake of ^{131}I-antiEGFR-BSA-PCL and ^{131}I-BSA-PCL, time activity measurements were obtained for the LS180 cell line. The radioiodide uptake in this cell line reached its maximum level after 4 h of incubation with ^{131}I-antiEGFR-BSA-PCL and ^{131}I-BSA-PCL. Furthermore, the ^{131}I uptake of ^{131}I-anti-EGFR-BSA-PCL was higher than that of ^{131}I-BSA-PCL. Cell-associated ^{131}I activity was still very high after 24 h and reached 79% to 84% in LS 180 cells because the liposomes had slow-release effects (Figure 2A). The CPM in the LS180 cells increased with an increasing dose of ^{131}I-labeled nanoparticles. However, radioactivity was maintained at a low level in the ^{131}I group (Figure 2B).

Growth curves for nude mice

The trend of body weight growth for all study groups is shown in Figure 3. The minimum reduction in body weight was found in the ^{131}I-antiEGFR-BSA-PCL and ^{131}I-BSA-PCL groups. Compared with the original body weight, mice treated with ^{131}I-antiEGFR-BSA-PCL, ^{131}I-BSA-PCL, ^{131}I, and normal saline demonstrated body weight losses of 39% ± 3%, 41% ± 4%, 49% ± 5%, and 55% ± 13%, respectively, on day 54 after

Figure 3 Changes in the animal body weight.

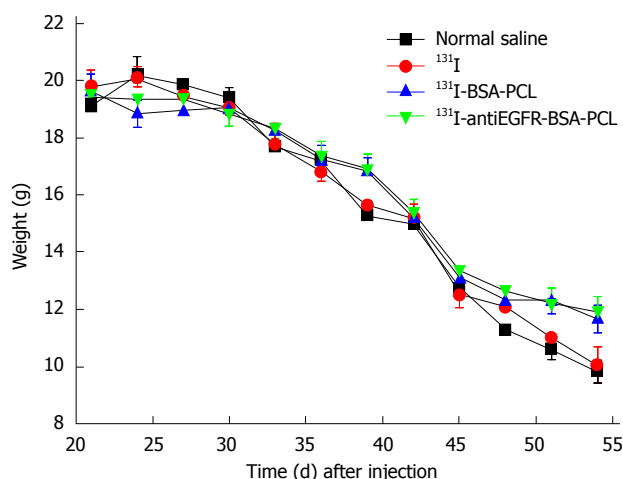**Figure 4 Changes in tumor volume.**

tumor inoculation ($P < 0.05$).

Tumor volume of nude mice

Rapid tumor growth was observed in the xenografted colorectal cancer nude mice treated with saline or ^{131}I. The tumor volume change is presented in Figure 4. By contrast, tumors grew slowly in mice treated with ^{131}I-antiEGFR-BSA-PCL or ^{131}I-BSA-PCL, and the growth curves of these test groups were similar. No significant differences were observed between the other two groups: those treated with ^{131}I or normal saline. The data showed that treatment with ^{131}I-antiEGFR-BSA-PCL and ^{131}I-BSA-PCL significantly inhibited tumor growth. At the end of the study, the volume of tumor increase in the ^{131}I-antiEGFR-BSA-PCL group was 124% ± 7%, which was lower than that of the ^{131}I-BSA-PCL (127% ± 9%), ^{131}I (143% ± 7%), and normal saline (146% ± 10%) groups. The results from the groups treated with ^{131}I-antiEGFR-BSA-PCL and ^{131}I-BSA-PCL were significantly different from those groups treated with ^{131}I and normal saline, suggesting that ^{131}I-antiEGFR-BSA-PCL and ^{131}I-BSA-PCL acted similarly to suppress tumor growth.

Tissue distribution of ^{131}I-antiEGFR-BSA-PCL, ^{131}I-BSA-PCL, and ^{131}I

The tissue distribution of ^{131}I-antiEGFR-BSA-PCL in nude mice with human colorectal cancer xenografts was measured by γ photon counts in Figure 5. ^{131}I-anti-EGFR-BSA-PCL was markedly taken up by tumor tissues. The tissue distribution assay revealed that ^{131}I-antiEGFR-BSA-PCL was markedly taken up by the tumor and reached its maximal uptake value of 21.0 ± 1.01 %ID/g at 72 h after the therapy. The drug concentration in the tumor was higher than those in the liver, heart, colon, or spleen at 72 h after therapy. Among the non-tumor tissues, ^{131}I-antiEGFR-BSA-PCL mostly accumulated in the liver and spleen. The levels of ^{131}I-antiEGFR-BSA-PCL and ^{131}I-BSA-PCL in tumor
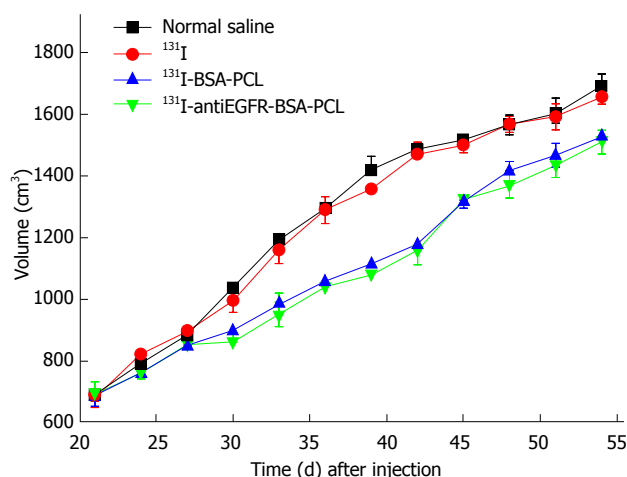
tissues were significantly higher than those observed in the ^{131}I group at 4, 24, and 72 h after treatment.

Histopathology

EGFR was overexpressed in the LS180 cell line (Figure 6), and the positive cell membranes were stained brown. The normal saline and ^{131}I-treated groups were characterized by well-developed proliferation of LS180 cells with a compact arrangement and diffusely distributed invading cancer nests; the nuclei were of various sizes and the staining color was variable. Moreover, no apparent necrosis was found in the cancer tissue (Figure 7). After the intratumoral injection of ^{131}I-antiEGFR-BSA-PCL and ^{131}I-BSA-PCL, xenografted colorectal cancer tissues were histopathologically examined (Figure 7). Upon comparison, a large field of the tumor tissue appeared necrotic. Evidence of dying tumor cells undergoing vacuolar degeneration of the cytoplasm was observed. Clusters of tumor cells decreased, whereas the intercellular space increased. Cellular arrangements were seen as discrete and not compact, and the cytoplasm was deeply stained. The cancerous nodes were characterized by patchy necrosis, and their tissue structure was smeared.

SPECT imaging

The SPECT images of LS180 tumor-bearing mice (21 d after tumor inoculation) were acquired at different time points after the intra-tumor injection of ^{131}I-antiEGFR-BSA-PCL, ^{131}I-BSA-PCL, and ^{131}I. The ^{131}I-antiEGFR-BSA-PCL and ^{131}I-BSA-PCL groups both exhibited slow blood clearance and maintained a relatively higher activity (primarily in the tumors, based on biodistribution data). Mice in the ^{131}I group had rapid blood clearance; their activity did not increase after 24 and 72 h compared with the ^{131}I-antiEGFR-BSA-PCL and ^{131}I-BSA-PCL groups. SPECT images showed high uptake and targeting of ^{131}I-antiEGFR-BSA-PCL and ^{131}I-BSA-PCL in the tumor. The results were correlated
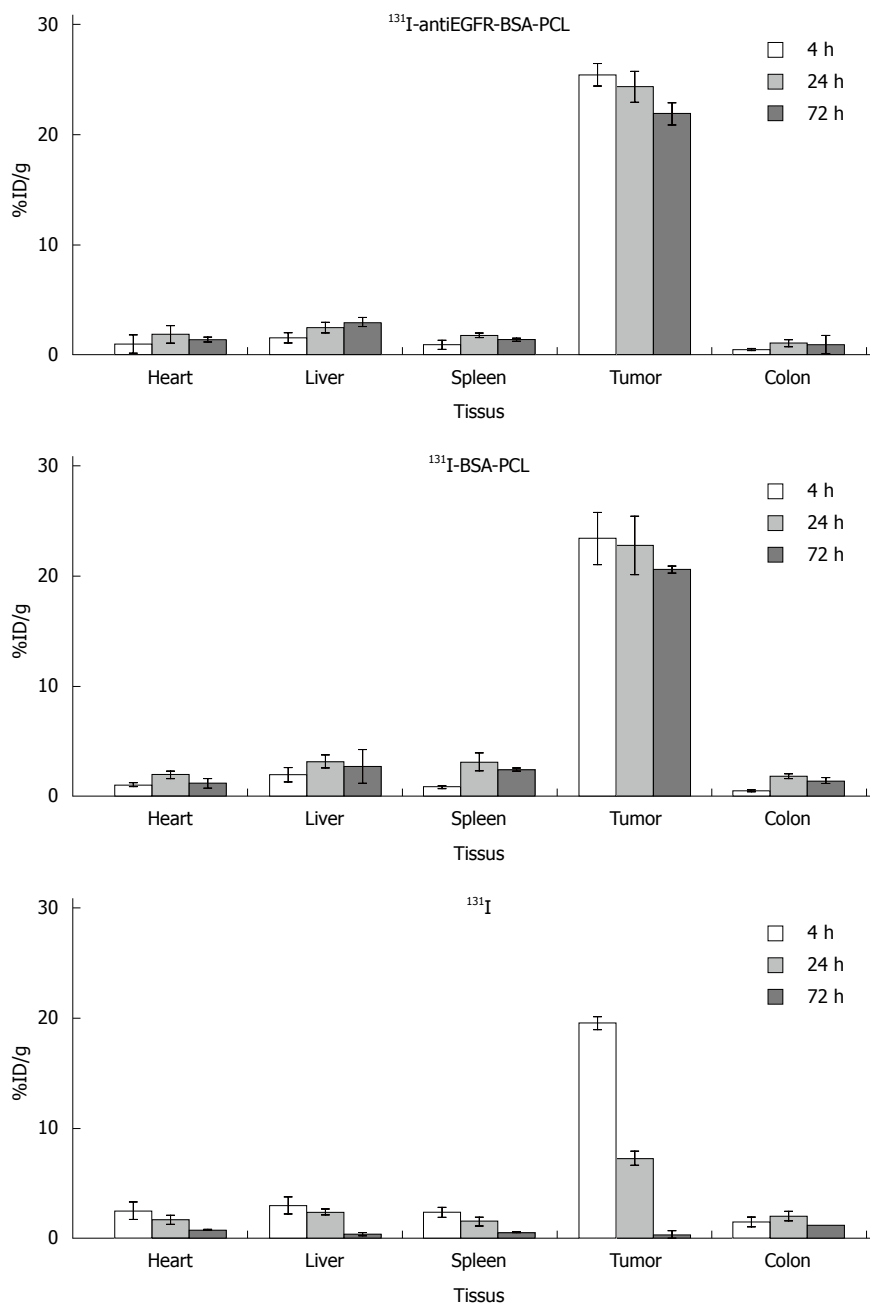
Figure 5 Tissue distribution of ^{131}I-antiEGFR-BSA-PCL, ^{131}I-BSA-PCL and [131]I.
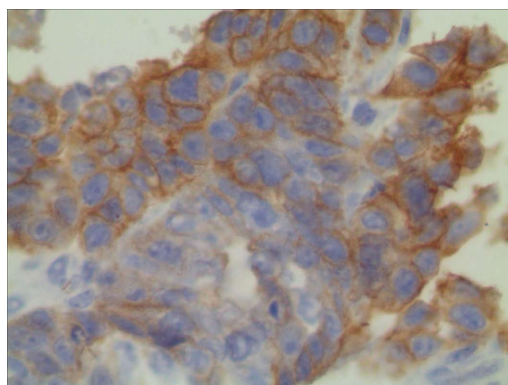
Figure 6 Immunohistochemical staining of LS180 colorectal cancer.

and validated with images of the biodistribution data.

DISCUSSION

Colorectal cancer is the third most common cancer worldwide[2]. The C26 murine colon carcinoma model has previously been reported to have a high level of metastasis that spreads after the intraperitoneal inoculation of tumor cells in BALB/c mice[20]. EGFR is a transmembrane receptor belonging to the ErbB family of receptors; the *EGFR* gene is activated or up-regulated in 60% to 80% of colorectal cancer cases[6,10]. Most of the normal tissues express very low levels of EGFR. However, the liver and kidney tissues

Figure 7 Histopathology of the liver, spleen, and tumor tissue at 3 d after the end of the treatment (× 100).
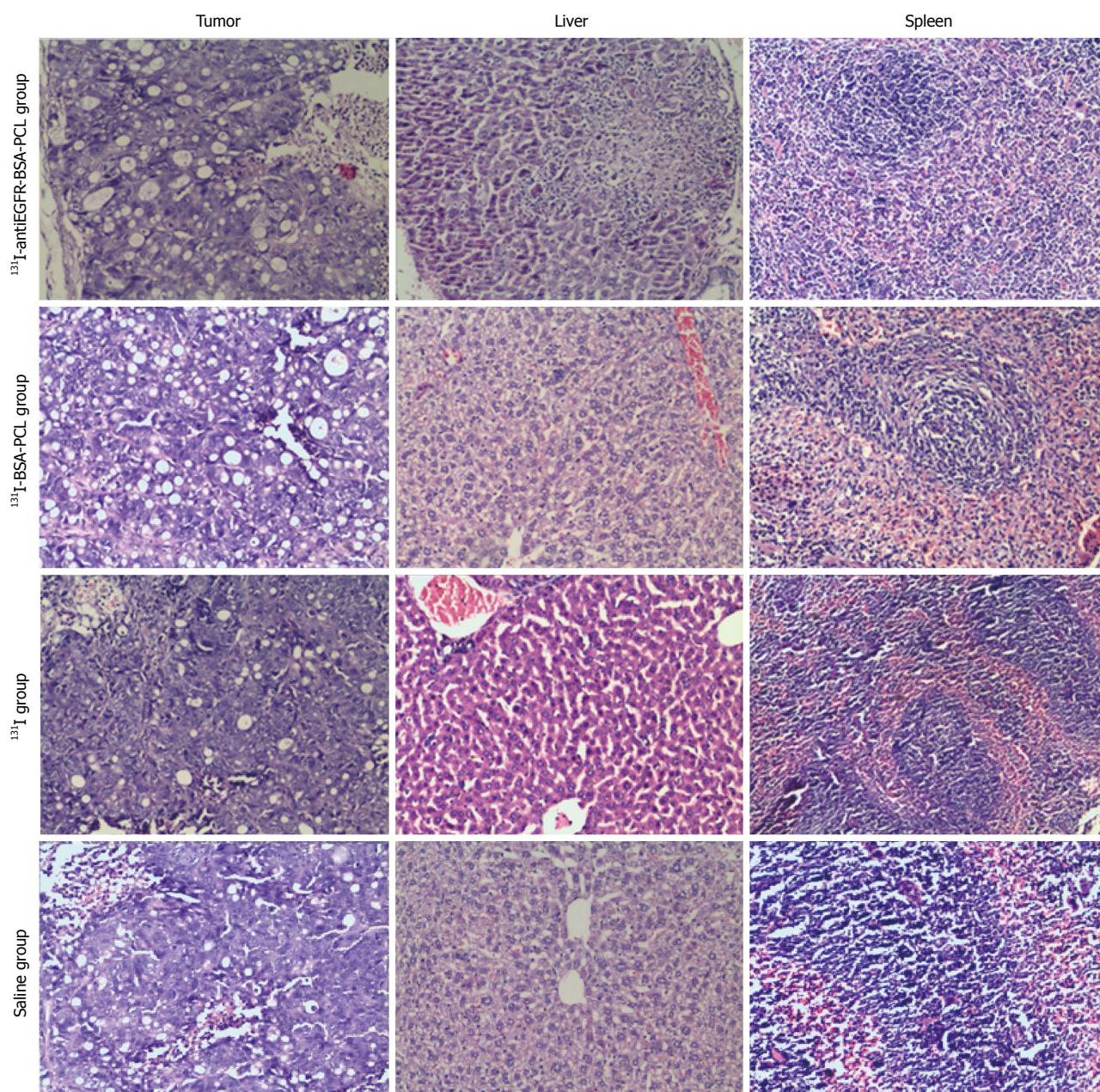
express moderately high levels of the receptor, which can exceed that of tumors.

Conventional anticancer drugs exhibit a lack of specificity, poor solubility and distribution, unfavorable pharmacokinetics, and high-tissue damage or toxicity[21]. Radiation therapy is typically delivered through high-energy external beam radiation to irradiate the cancerous tissue. Liposomes are spherical vesicles formed by lipid bilayers. These structures have been widely investigated as carriers of tumor-targeting therapy. Radioisotopes can be trapped within the inner space of the liposome, intercalated into the double membrane of the liposome, and connected with the surface of the liposome[22,23]. However, given the close proximity of critical organs to the tumor, the

delivery of a therapeutic dose of irradiation without causing serious complications is often impossible, even with technological advancements in radiation dose distribution, such as intensity-modulated radiation therapy[24,25]. Tumor-targeting therapy has overcome the lack of specificity of traditional therapeutic agents. Recent work comparing non-targeted and targeted nanoparticles (lipid-based[26] or polymer-based[27]) has shown that the primary role of the targeting ligands is to enhance the cellular uptake of drugs by cancer cells rather than to increase their accumulation in the tumor. Kao *et al*[12] demonstrated the enhanced endocytosis and cytotoxicity of ^{131}I-C225-AuNP-PEG against EGFR-overexpressing human A549 lung carcinoma cells as well as its active targeting in an A549 tumor xenograft

mouse model[12].

Chen *et al*[28] and Chang *et al*[19] reported the biodistribution, pharmacokinetics, and micro-SPECT/CT imaging of the [188]Re-liposome in C26 colon carcinoma ascites and solid tumor animal models. Their results demonstrated the potential benefit and advantages of the [188]Re-liposome in the C26 animal model. Bao *et al*[29] reported that the intratumoral injection of liposomal radionuclides had a slower clearance rate. [131]I is a radionuclide with a gamma emission of 364 keV (81.7%) and a beta emission of 0.606 MeV (89.9%). This molecule has the advantages of imaging feasibility and beta-emitting therapeutic effects. In the present study, the initial treatment of colorectal cancer with ^{131}I-antiEGFR-BSA-PCL reduced the risk of disease progression compared with ^{131}I-BSA-PCL and [131]I. The decreased risk was evidenced by changes in the tumor volume, mouse survival time, and mouse weight. As shown by the data, the rates of increase of the final tumor volumes in the groups treated with ^{131}I-antiEGFR-BSA-PCL and ^{131}I-BSA-PCL were lower than those of tumor-bearing groups treated with ^{131}I and normal saline**.** However, the tumor volumes of the group treated with normal saline and the group treated with ^{131}I were not significantly different in terms of overall survival. The trend of the body weight growth also had the same characteristics. The ^{131}I-antiEGFR-BSA-PCL group also achieved the maximum suppression of tumor growth, which reflected an enhancement of cancer therapy with the use of ^{131}I-antiEGFR-BSA-PCL. We found that the use of ^{131}I-antiEGFR-BSA-PCL for the *in vivo* therapy of colorectal cancer was both feasible and reliable, with favorable *in vivo* characteristics.

Results with mouse models demonstrated the steady extravasation of nanoliposomes into ascites with the gradual release of the drug, followed by drug diffusion into the tumor cellular compartment[30,31]. Wang *et al*[32] reported that direct intratumoral drug administration in advanced neck and head tumors was clearly appealing and immediately achieved high drug concentrations at the target sites without the associated side effects of external beam radiation or systemic chemotherapy. Their group also proved that direct injection could deliver drugs into areas of the tumor that had high interstitial pressure and large areas of avascular necrosis. This study was relevant to the present study on the pharmacokinetics and effectiveness of ^{131}I-antiEGFR-BSA-PCL administration in the heart, liver, spleen, colon, and tumor cells. The observed iodine uptake demonstrated the potential benefits and advantages of ^{131}I-antiEGFR-BSA-PCL in the LS180 animal model. The accumulation of radioactivity in the tumor was maintained at steady levels for at least 24 h.

SPECT imaging is a non-invasive imaging modality that can monitor the behavior of radiotherapeutics in the same animal at different time points. After the injection of different drugs, the SPECT imaging and iodine uptake showed that the tumor uptake of

[131]I-antiEGFR-BSA-PCL and ^{131}I-BSA-PCL was obvious higher than that of [131]I. In addition, the *in vitro* stability of the passive ^{131}I-antiEGFR-BSA-PCL was found to be higher after 24 h of inoculation. Some mice presented skin ulcerations at around day 13 but were healed by day 19. From the SPECT fusion images, we noticed that the ^{131}I-antiEGFR-BSA-PCL had the tendency to spread into the tumor, liver, spleen, and urinary bladder area. We also observed that the non-tumor tissues of the liver and spleen, which are reticuloendothelial system-rich organs, exhibited significant uptake of ^{131}I-antiEGFR-BSA-PCL and ^{131}I-BSA-PCL. The remarkable accumulation of these compounds in the bladder implied that renal clearance is the predominant route of excretion of radioactive metabolites. A glutathione-coated luminescent gold nanoparticle (3 nm diameter)[33] and a gadolinium-loaded dendrimer-entrapped gold nanoparticle (90 nm mean diameter)[34] were previously reported to be excreted *via* the urinary system. Li *et al*[16] showed that ^{131}I-labeled rhEGF was markedly absorbed by tumor tissue in xenografted nude mice and reached a maximum uptake rate (16.73 %ID/g) at 120 h after intravenous injection. Their group suggested that ^{131}I-labeled rhEGF could be absorbed by breast cancer tissues and might be a useful clinical candidate. Data from the present study also showed a low immediate clearance for both ^{131}I-antiEGFR-BSA-PCL and ^{131}I-BSA-PCL. The long phase was observed at 72 h after ^{131}I-antiEGFR-BSA-PCL and ^{131}I-BSA-PCL were injected, thereby translating to a high locoregional retention rate when the immediate clearance period had passed. These data supported the notion that the injection of liposomal radionuclides could lead to higher retention rates.

The anti-tumor effect of ^{131}I-antiEGFR-BSA-PCL could also be seen in the histopathological studies. Immunohistochemistry showed that the LS180 cell line overexpressed EGFR. The normal saline and ^{131}I-treated groups were characterized by well-developed proliferation of LS180 cells and diffusely distributed invading cancer nests. No apparent necrosis was observed in the cancer tissue. In the xenografted colorectal cancer tissues of the groups treated with ^{131}I-antiEGFR-BSA-PCL and ^{131}I-BSA-PCL, a large field of the tumor tissue appeared necrotic. Evidence of dying tumor cells undergoing vacuolar degeneration of the cytoplasm was observed. The cancerous nodes were characterized by patchy necrosis, and the tissue structures were smeared. These results demonstrated that treatment with ^{131}I-antiEGFR-BSA-PCL and ^{131}I-BSA-PCL led to histopathological changes in colorectal cancer tissue that were associated with the death of the tumor cells. The above-mentioned reasons made the intraoperative injection of liposomal therapeutic radionuclides a particularly effective treatment option for advanced colorectal cancer.

Although the colorectal cancer xenografted animal model used in this study was not orthotopic, the

results are still valuable for interpreting the drug efficiency of ^{131}I-antiEGFR-BSA-PCL and ^{131}I-BSA-PCL. Therefore, the protocols used in this study revealed that the designed formulation and treatment trials were novel for a preclinical study.

In conclusion, the results of this study demonstrated that ^{131}I-antiEGFR-BSA-PCL and ^{131}I-BSA-PCL had superior cellular binding and higher cellular uptake compared with [131]I *in vitro* and *in vivo*. ^{131}I-antiEGFR-BSA-PCL suppressed the development of tumors and exhibited pronounced anti-proliferation ability against the xenografted LS180 cells in a mouse model, as demonstrated by changes in the tumor size, body weight, histopathology, and SPECT imaging. This study revealed that ^{131}I-antiEGFR-BSA-PCL was effective in the killing of tumors, but we did not observe a radiation induced breakdown of the kidney and liver. Therefore, ^{131}I-antiEGFR-BSA-PCL may be a safe drug for radiotherapy in colorectal cancer.

COMMENTS

Background
Epidermal growth factor receptor (EGFR) is a cell-surface receptor that plays a key role in signaling pathways. Such pathways regulate cell proliferation, angiogenesis, and tumor metastases. EGFR is widely overexpressed in several tumor types, including breast cancer, melanoma, brain glioblastoma, non-small cell lung cancer, and colorectal cancer. EGFR is an attractive candidate for anti-cancer therapy.

Research frontiers
Previous experiments have already proven that EGFR is widely overexpressed in colorectal cancer.

Innovations and breakthroughs
This is the first study evaluating the cellular binding and cellular uptake of ^{131}I-antiEGFR-BSA-PCL and ^{131}I-BSA-PCL *in vitro* and *in vivo*. ^{131}I-antiEGFR-BSA-PCL suppressed the development of tumors and exhibited pronounced anti-proliferation ability against the xenografted LS180 cells in a mouse model.

Applications
As a novel theranostic agent, ^{131}I-antiEGFR-BSA-PCL exhibited pronounced anti-tumoral effects on colorectal cancer.

Peer-review
This study evaluated the therapeutic effectiveness of ^{131}I-antiEGFR-BSA-PCL in the colorectal cancer mouse model and demonstrated the potential beneficial application of ^{131}I-antiEGFR-BSA-PCL for treating colorectal cancer. The manuscript is well written and properly conducted.

REFERENCES

1   **Fang M**, Peng CW, Pang DW, Li Y. Quantum dots for cancer research: current status, remaining issues, and future perspectives. *Cancer Biol Med* 2012; **9**: 151-163 [PMID: 23691472 DOI: 10.7497/j.issn.2095-3941.2012.03.001]

2   **Parkin DM**, Bray F, Ferlay J, Pisani P. Global cancer statistics, 2002. *CA Cancer J Clin* 2005; **55**: 74-108 [PMID: 15761078 DOI: 10.3322/canjclin.55.2.74]

3   **Gabizon A**, Shmeeda H, Barenholz Y. Pharmacokinetics of pegylated liposomal Doxorubicin: review of animal and human studies. *Clin Pharmacokinet* 2003; **42**: 419-436 [PMID: 12739982 DOI: 10.2165/00003088-200342050-00002]

4   **Allen TM**, Cullis PR. Drug delivery systems: entering the mainstream. *Science* 2004; **303**: 1818-1822 [PMID: 15031496 DOI: 10.1126/science.1095833]

5   **Mendelsohn J**, Baselga J. The EGF receptor family as targets for cancer therapy. *Oncogene* 2000; **19**: 6550-6565 [PMID: 11426640 DOI: 10.1038/sj.onc.1204082]

6   **Messa C**, Russo F, Caruso MG, Di Leo A. EGF, TGF-alpha, and EGF-R in human colorectal adenocarcinoma. *Acta Oncol* 1998; **37**: 285-289 [PMID: 9677101 DOI: 10.1080/028418698429595]

7   **Ciardiello F**, Tortora G. EGFR antagonists in cancer treatment. *N Engl J Med* 2008; **358**: 1160-1174 [PMID: 18337605 DOI: 10.1056/NEJMra0707704]

8   **Yang J**, Lim EK, Lee HJ, Park J, Lee SC, Lee K, Yoon HG, Suh JS, Huh YM, Haam S. Fluorescent magnetic nanohybrids as multimodal imaging agents for human epithelial cancer detection. *Biomaterials* 2008; **29**: 2548-2555 [PMID: 18329706 DOI: 10.1016/j.biomaterials.2007.12.036]

9   **Nurwidya F**, Murakami A, Takahashi F, Takahashi K. Molecular mechanisms contributing to resistance to tyrosine kinase-targeted therapy for non-small cell lung cancer. *Cancer Biol Med* 2012; **9**: 18-22 [PMID: 23691449 DOI: 10.3969/j.issn.2095-3941.2012.01.003]

10 **Porebska I**, Harlozińska A, Bojarowski T. Expression of the tyrosine kinase activity growth factor receptors (EGFR, ERB B2, ERB B3) in colorectal adenocarcinomas and adenomas. *Tumour Biol* 2000; **21**: 105-115 [PMID: 10686540]

11 **Koppe MJ**, Bleichrodt RP, Soede AC, Verhofstad AA, Goldenberg DM, Oyen WJ, Boerman OC. Biodistribution and therapeutic efficacy of (125/131)I-, (186)Re-, (88/90)Y-, or (177)Lu-labeled monoclonal antibody MN-14 to carcinoembryonic antigen in mice with small peritoneal metastases of colorectal origin. *J Nucl Med* 2004; **45**: 1224-1232 [PMID: 15235070]

12 **Kao HW**, Lin YY, Chen CC, Chi KH, Tien DC, Hsia CC, Lin MH, Wang HE. Evaluation of EGFR-targeted radioimmuno-gold-nanoparticles as a theranostic agent in a tumor animal model. *Bioorg Med Chem Lett* 2013; **23**: 3180-3185 [PMID: 23628334 DOI: 10.1016/j.bmcl.2013.04.002]

13 **Su CH**, Sheu HS, Lin CY, Huang CC, Lo YW, Pu YC, Weng JC, Shieh DB, Chen JH, Yeh CS. Nanoshell magnetic resonance imaging contrast agents. *J Am Chem Soc* 2007; **129**: 2139-2146 [PMID: 17263533 DOI: 10.1021/ja0672066]

14 **Liu Z**, Dong C, Wang X, Wang H, Li W, Tan J, Chang J. Self-assembled biodegradable protein-polymer vesicle as a tumor-targeted nanocarrier. *ACS Appl Mater Interfaces* 2014; **6**: 2393-2400 [PMID: 24456410 DOI: 10.1021/am404734c]

15 **Ickenstein LM**, Edwards K, Sjöberg S, Carlsson J, Gedda L. A novel 125I-labeled daunorubicin derivative for radionuclide-based cancer therapy. *Nucl Med Biol* 2006; **33**: 773-783 [PMID: 16934696]

16 **Li YC**, Xu WY, Tan TZ, He S. 131I-recombinant human EGF has antitumor effects against MCF-7 human breast cancer xenografts with low levels of EGFR. *Nucl Med Biol* 2004; **31**: 435-440 [PMID: 15093813 DOI: 10.1016/j.nucmedbio.2003.11.010]

17 **Shao X**, Zhang H, Rajian JR, Chamberland DL, Sherman PS, Quesada CA, Koch AE, Kotov NA, Wang X. 125I-labeled gold nanorods for targeted imaging of inflammation. *ACS Nano* 2011; **5**: 8967-8973 [PMID: 22003968 DOI: 10.1021/nn203138t]

18 **Lee YS**, Bullard DE, Zalutsky MR, Coleman RE, Wikstrand CJ, Friedman HS, Colapinto EV, Bigner DD. Therapeutic efficacy of antiglioma mesenchymal extracellular matrix 131I-radiolabeled murine monoclonal antibody in a human glioma xenograft model. *Cancer Res* 1988; **48**: 559-566 [PMID: 2446747]

19 **Chang YJ**, Chang CH, Chang TJ, Yu CY, Chen LC, Jan ML, Luo TY, Lee TW, Ting G. Biodistribution, pharmacokinetics and microSPECT/CT imaging of 188Re-bMEDA-liposome in a C26 murine colon carcinoma solid tumor animal model. *Anticancer Res* 2007; **27**: 2217-2225 [PMID: 17695506]

20 **Corbett TH**, Griswold DP, Roberts BJ, Peckham JC, Schabel FM. Evaluation of single agents and combinations of chemotherapeutic agents in mouse colon carcinomas. *Cancer* 1977; **40**: 2660-2680 [PMID: 922705 DOI: 10.1002/1097-0142(197711)40:5]

21   **Ting G**, Chang CH, Wang HE, Lee TW. Nanotargeted radionu- clides for cancer nuclear imaging and internal radiotherapy. *J Biomed Biotechnol* 2010; **2010**: pii 953537 [PMID: 20811605 DOI: 10.1155/2010/953537]

22   **Bao A**, Goins B, Klipper R, Negrete G, Phillips WT. Direct 99mTc labeling of pegylated liposomal doxorubicin (Doxil) for pharmacokinetic and non-invasive imaging studies. *J Pharmacol Exp Ther* 2004; **308**: 419-425 [PMID: 14610219 DOI: 10.1124/ jpet.103.059535]

23   **Bao A**, Goins B, Klipper R, Negrete G, Phillips WT. 186Re- liposome labeling using 186Re-SNS/S complexes: in vitro stability, imaging, and biodistribution in rats. *J Nucl Med* 2003; **44**: 1992-1999 [PMID: 14660726]

24   **Lee N**, Puri DR, Blanco AI, Chao KS. Intensity-modulated radiation therapy in head and neck cancers: an update. *Head Neck* 2007; **29**: 387-400 [PMID: 16358297 DOI: 10.1002/hed.20332]

25   **Xia P**, Fu KK, Wong GW, Akazawa C, Verhey LJ. Comparison of treatment plans involving intensity-modulated radiotherapy for nasopharyngeal carcinoma. *Int J Radiat Oncol Biol Phys* 2000; **48**: 329-337 [PMID: 10974445 DOI: 10.1016/S0360- 3016(00)00585-X]

26   **Kirpotin DB**, Drummond DC, Shao Y, Shalaby MR, Hong K, Nielsen UB, Marks JD, Benz CC, Park JW. Antibody targeting of long- circulating lipidic nanoparticles does not increase tumor localization but does increase internalization in animal models. *Cancer Res* 2006; **66**: 6732-6740 [PMID: 16818648 DOI: 10.1158/0008-5472. CAN-05-4199]

27   **Bartlett DW**, Su H, Hildebrandt IJ, Weber WA, Davis ME. Impact of tumor-specific targeting on the biodistribution and efficacy of siRNA nanoparticles measured by multimodality in vivo imaging. *Proc Natl Acad Sci USA* 2007; **104**: 15549-15554 [PMID: 17875985 DOI: 10.1073/pnas.0707461104]

28   **Chen LC**, Chang CH, Yu CY, Chang YJ, Wu YH, Lee WC, Yeh CH, Lee TW, Ting G. Pharmacokinetics, micro-SPECT/CT imaging and therapeutic efficacy of (188)Re-DXR-liposome in C26 colon carcinoma ascites mice model. *Nucl Med Biol* 2008; **35**: 883-893 [PMID: 19026950 DOI: 10.1016/j.nucmedbio.2008.09.005]

29   **Bao A**, Phillips WT, Goins B, Zheng X, Sabour S, Natarajan M, Ross Woolley F, Zavaleta C, Otto RA. Potential use of drug carried-liposomes for cancer therapy via direct intratumoral injection. *Int J Pharm* 2006; **316**: 162-169 [PMID: 16580161 DOI: 10.1016/j.ijpharm.2006.02.039]

30   **Bally MB**, Masin D, Nayar R, Cullis PR, Mayer LD. Transfer of liposomal drug carriers from the blood to the peritoneal cavity of normal and ascitic tumor-bearing mice. *Cancer Chemother Pharmacol* 1994; **34**: 137-146 [PMID: 8194164 DOI: 10.1007/ BF00685931]

31   **Gabizon AA**. Selective tumor localization and improved therapeutic index of anthracyclines encapsulated in long-circulating liposomes. *Cancer Res* 1992; **52**: 891-896 [PMID: 1737351]

32   **Wang SX**, Bao A, Herrera SJ, Phillips WT, Goins B, Santoyo C, Miller FR, Otto RA. Intraoperative 186Re-liposome radionuclide therapy in a head and neck squamous cell carcinoma xenograft positive surgical margin model. *Clin Cancer Res* 2008; **14**: 3975-3983 [PMID: 18559620 DOI: 10.1158/1078-0432.CCR-07-4149]

33   **Zhou C**, Hao G, Thomas P, Liu J, Yu M, Sun S, Öz OK, Sun X, Zheng J. Near-infrared emitting radioactive gold nanoparticles with molecular pharmacokinetics. *Angew Chem Int Ed Engl* 2012; **51**: 10118-10122 [PMID: 22961978 DOI: 10.1002/anie.201203031]

34   **Wen S**, Li K, Cai H, Chen Q, Shen M, Huang Y, Peng C, Hou W, Zhu M, Zhang G, Shi X. Multifunctional dendrimer-entrapped gold nanoparticles for dual mode CT/MR imaging applications. *Biomaterials* 2013; **34**: 1570-1580 [PMID: 23199745 DOI: 10.1016/j.biomaterials.2012.11.010]

Baishideng®